HHS Public Access

Author manuscript

*Cell Rep*. Author manuscript; available in PMC 2018 March 28.

Published in final edited form as:

*Cell Rep*. 2018 March 06; 22(10): 2601–2614. doi:10.1016/j.celrep.2018.01.075.

# Retinal Cell Type DNA Methylation and Histone Modifications Predict Reprogramming Efficiency and Retinogenesis in 3D Organoid Cultures

**Lu Wang**[1,8], **Daniel Hiler**[1,8], **Beisi Xu**[2,8], **Issam AlDiri**[1], **Xiang Chen**[2], **Xin Zhou**[2], **Lyra Griffiths**[1], **Marc Valentine**[4], **Abbas Shirinifard**[1], **András Sablauer**[3], **Suresh Thiagarajan**[3], **Marie-Elizabeth Barabas**[1], **Jiakun Zhang**[1], **Dianna Johnson**[6], **Sharon Frase**[5], and **Michael A. Dyer**[1,6,7,9,*]

[1]Department of Developmental Neurobiology, St. Jude Children's Research Hospital, Memphis, TN 38105, USA

[2]Department of Computational Biology, St. Jude Children's Research Hospital, Memphis, TN 38105, USA

[3]Department of Diagnostic Imaging, St. Jude Children's Research Hospital, Memphis, TN 38105, USA

[4]Cytogenetics Shared Resource, St. Jude Children's Research Hospital, Memphis, TN 38105, USA

[5]Cell and Tissue Imaging Shared Resource, St. Jude Children's Research Hospital, Memphis, TN 38105, USA

[6]Department of Ophthalmology, University of Tennessee Health Science Center, Memphis, TN 38163, USA

[7]Howard Hughes Medical Institute, Chevy Chase, MD 20815, USA

## SUMMARY



*Correspondence: michael.dyer@stjude.org.
[8]These authors contributed equally
[9]Lead Contact

**DATA AND SOFTWARE AVAILABILITY**

The accession number for the data reported in this paper is GEO: GSE87064. All the data are also hosted on a free online viewer at https://pecan.stjude.org/proteinpaint/study/retinaliPSC2017.

**SUPPLEMENTAL INFORMATION**

Supplemental Information includes Supplemental Experimental Procedures, three figures, and 11 tables and can be found with this article online at https://doi.org/10.1016/j.celrep.2018.01.075.

**AUTHOR CONTRIBUTIONS**

Conceptualization, M.A.D., D.H., and L.W.; Methodology, B.X., X.C., M.V., A. Shirinifard, and S.T.; Formal Analysis, M.A.D., D.H., B.X., X.C., X.Z., and A. Shirinifard; Investigation, M.A.D., D.H., L.W., M.V., L.G., J.Z., D.J., S.F., I.A., and M.-E.B.; Writing, M.A.D.; Supervision, M.A.D., A. Sablauer, and X.C.; Project Administration, M.A.D.; Funding Acquisition, M.A.D.

**DECLARATION OF INTERESTS**

The authors declare no competing interests.

Diverse cell types can be reprogrammed into pluripotent stem cells by ectopic expression of Oct4 (Pou5f1), Klf4, Sox3, and Myc. Many of these induced pluripotent stem cells (iPSCs) retain memory, in terms of DNA methylation and histone modifications (epigenetic memory), of their cellular origins, and this may bias subsequent differentiation. Neurons are difficult to reprogram, and there has not been a systematic side-by-side characterization of reprogramming efficiency or epigenetic memory across different neuronal subtypes. Here, we compare reprogramming efficiency of five different retinal cell types at two different stages of development. Retinal differentiation from each iPSC line was measured using a quantitative standardized scoring system called STEM-RET and compared to the epigenetic memory. Neurons with the lowest reprogramming efficiency produced iPSC lines with the best retinal differentiation and were more likely to retain epigenetic memory of their cellular origins. In addition, we identified biomarkers of iPSCs that are predictive of retinal differentiation.

## Graphical abstract

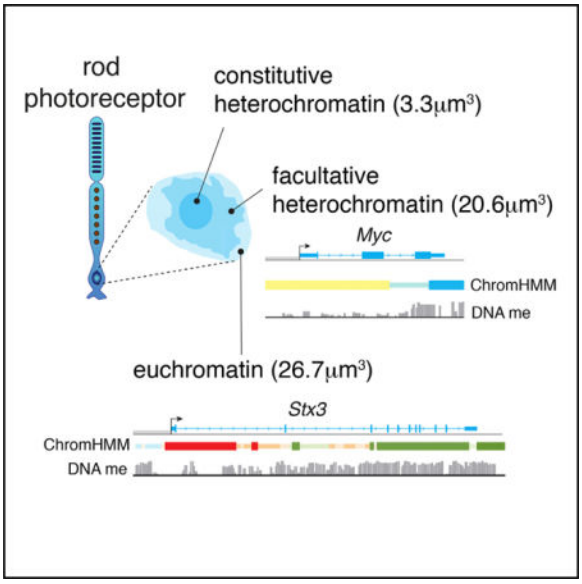


## INTRODUCTION

Somatic cells can be reprogrammed to multipotent stem cells by ectopic expression of defined factors (Oct4, Klf4, Sox2, and Myc), which holds great promise for patient-specific disease modeling and regenerative medicine (Chen et al., 2015; Dyer, 2016; Singh et al., 2015). In addition to the fibroblasts that were used in the first successful reprogramming experiments (Takahashi et al., 2007; Yu et al., 2007), a myriad of other cell types have been reprogrammed into induced pluripotent stem cells (iPSCs) (Aoi et al., 2008; Lowry et al., 2008; Park et al., 2008). Reprogramming efficiency is cell type specific and is thought to be stochastic for any homogeneous population of cells (Hanna et al., 2009). Bone-marrow-derived hematopoietic stem cells have some of the highest rates of reprogramming (28%) (Eminli et al., 2009), and mature differentiated neurons are among the most difficult to reprogram (Hiler et al., 2015, 2016; Kim et al., 2011). Indeed, early attempts to reprogram murine cortical neurons failed to produce iPSCs, unless the *p53* gene was inactivated (Kim

et al., 2011). More recently, an alternative approach was developed to reprogram neurons with wild-type *p53* (Hiler et al., 2015, 2016).

iPSCs derived from diverse cell types have been shown to harbor epigenetic memory of their cellular origins that makes them more or less likely to differentiate along particular lineages (Bar-Nur et al., 2011; Kim et al., 2010; Polo et al., 2010). In some iPSC lines, this epigenetic memory is gradually depleted with passage in culture, but in other examples, it is stably maintained (Kim et al., 2010, 2011; Nishino et al., 2011; Polo et al., 2010). The majority of studies on epigenetic memory in iPSCs have focused on DNA methylation, but recent evidence suggests that it may also extend to other epigenomic factors such as histone modifications at promoters and gene bodies and higher order chromatin organization with topologically associated domains (TADs) mediated by CTCF (Beagan et al., 2016; Krijger et al., 2016). It is not known how reprogramming efficiency relates to epigenetic memory, nor is it known how the dynamic changes in the epigenome, which occur as cells differentiate, relate to epigenetic memory and cellular reprogramming.

In this study, we compare the reprogramming efficiency of 5 cell types in the retina at two stages of development and relate that to the ability of these retinal-derived iPSCs (r-iPSCs) to subsequently differentiate into retina. The cells that were most difficult to reprogram made the best retina, as determined by STEM-RET scoring (Hiler et al., 2015, 2016), and this was reflected in their epigenetic memory. Moreover, characterization of a series of lines that failed to produce retina from diverse sources identified epigenetic features of several genes, including *Meis1* target genes that are predictive of retinogenesis for stem cells. This work will have implications for the selection of cell populations for cell-based therapy and for using reprogramming of purified cell populations to advance our understanding of the role of the epigenome in normal differentiation.

## RESULTS

### Cell Type Specification and Developmental Stage Influence Reprogramming Efficiency in the Retina

We have previously demonstrated the feasibility of reprogramming rod photoreceptors using the *Nrl-GFP;Col1a1-OKSM;Rosa26-M2rtTA* mouse strain (Hiler et al., 2015, 2016) (Figure 1A). To extend our previous studies and compare the reprogramming efficiency across retinal cell types, we generated 4 additional mouse lines by crossing GFP transgenic mice with the *Col1a1-OKSM;Rosa26-M2rtTA* strain (Stadtfeld et al., 2010). The *Chrnb4-GFP* transgene labels cone photoreceptors (Figure 1B) (Siegert et al., 2009), *Rlbp1-GFP* labels Müller glia (Figure 1C) (Vázquez-Chona et al., 2009), *Gad1-GFP* labels horizontal and a subset of amacrine interneurons (Figure 1D) (Huckfeldt et al., 2009), and *Grm6-GFP* labels ON bipolar cells (Figure 1E) (Dhingra et al., 2008). Next, we used a serial limiting dilution procedure in retinal pellets to quantitate reprogramming efficiency (Hiler et al., 2015, 2016). Briefly, GFP+ cells from the different reprogrammable mouse strains were mixed with $1.5 \times 10^6$ C57BL/6 post-natal day (P)0–P5 retinal cells in retinal pellets and cultured on polycarbonate filters in retinal explant culture medium (Hiler et al., 2015, 2016). This procedure is essential, because purified mature retinal neurons do not survive when cultured on plastic or on irradiated mouse embryonic fibroblasts (MEFs). The reprogrammable cells

were mixed with the normal retinal cells in these retinal pellets in limiting dilutions (20,000, 2,000, or 200 cells per pellet) (Supplemental Information). Doxycycline (2 μg/mL) was added to the pellet cultures to induce expression of *Oct3/4 (Pou5f1)*, *Klf4*, *Sox2*, and *Myc* (*OKSM)* in the reprogrammable neurons for 10 days. Then, individual pellets were dissociated and plated in limiting dilution on irradiated MEFs in the presence of leukemia inhibitor factor (LIF) to support the growth of iPSC colonies (Supplemental Information). We used mature (P21) and immature (P2–P5) cells for each cell type, and 2–3 independent reprogramming experiments were performed for each cell type at each stage of development. We also generated fibroblast-derived iPSCs from the same mouse lines as those used for retinal reprogramming for comparison to the retinal derived iPSCs.

We calculated the reprogramming efficiency (see Supplemental Information) for MEFs and each of the 5 cell types at each developmental stage and calculated the mean and SD across multiple independent experiments (Figures 1F–1J). Mature rod photoreceptors had a significantly lower reprogramming efficiency ($p < 0.01$) relative to cones, Müller glia, amacrine/horizontal interneurons, and immature rod photoreceptors (Figures 1F–1J). The most efficient reprogramming was achieved with Müller glia and interneurons (amacrine/horizontal neurons), and the lowest reprogramming efficiency was achieved with bipolar neurons (Figures 1F–1J).

We isolated and grew lines to passage 20 prior to characterization. Using molecular and cellular markers, we identified lines that underwent complete reprogramming and maintained a stable karyotype as described previously (Figures 1K–1O; Supplemental Information) (Hiler et al., 2015, 2016). We selected 59 lines for subsequent analyses, including the 8 rod-derived iPSC lines that were previously described (Table S1) (Hiler et al., 2015).

## Nuclear Organization and Localization of Pluripotency Genes in Retinal Cell Types

One of the key steps to cellular reprogramming is reversing the epigenetic marks that accumulate during differentiation and activation of the endogenous pluripotency genes (Apostolou and Hochedlinger, 2013). This is particularly important in the retina because of the cell-type-specific 3-dimensional (3D) organization of the chromatin in the nucleus (Chen et al., 2015; Dyer, 2016; Solovei et al., 2009) (Figures 2A and 2B). To determine whether there was an inverse correlation between the proportion of heterochromatin in the nuclei and reprogramming efficiency, we performed serial block face imaging on the FEI Teneo electron microscope to produce 3D datasets on each of the 5 classes of retinal cell types used in this study in triplicate (rods, cones, bipolar cells, Müller glia, and amacrine cells) (Figure 2B). Next, we developed an algorithm to segment the heterochromatin and euchromatin based on image features in the 3D electron microscopy (EM) datasets (Supplemental Information). Rod photoreceptors have the smallest nuclei with the largest amount of heterochromatin, while the bipolar neurons have the largest nuclei with the least heterochromatin in our analysis (Figures 2B and 2C).

Next, to determine where in the nucleus the reprogramming genes were located, we performed fluorescence *in situ* hybridization (FISH) of *Oct4*, *Klf4*, *Sox2*, and *Myc* on adult retina and performed 3D reconstruction of individual nuclei using confocal microscopy. To

identify the euchromatin in each nucleus, we performed immunostaining for H3K4me3 prior to hybridization of the FISH probes (Figures 2D and 2E). The facultative hetero-chromatin (f-het) and constitutive heterochromatin (c-het) can be distinguished by DAPI staining intensity. In mature rods, *Oct4* was localized in the euchromatin, and *Myc* was in the f-heterochromatin domain (Figures 2D and 2E). *Sox2* and *Klf4* were also in the f-heterochromatin domain in rods, but they were at the boundary with euchromatin (Figure 2F). In the other cell types, all 4 genes were localized to the euchromatin domain (Figures 2G and 2H).

To relate their 3D position within the nucleus to their 1D epigenetic state, we analyzed chromatin immunoprecipitation sequencing (ChIP-seq) for 8 histone marks, CTCF, Brd4 and RNA polymerase II (Pol II), DNA methylation, assay for transposable-accessible chromatin sequencing (ATAC-seq), and RNA sequencing (RNA-seq) data for adult retina (data available at https://pecan.stjude.org/proteinpaint/study/retina2017; Aldiri et al., 2017). To integrate the individual ChIP-seq tracks, we performed chromatin hidden Markov modeling (chromHMM) using 11 chromHMM states, as done previously for murine retina (Figure 2I) (Aldiri et al., 2017).

In the adult retina, *Oct4, Klf4*, and *Myc* are not expressed (fragments per kilobase per million mapped reads [FPKM] < 1.0), and *Sox2* is expressed at low levels (FPKM < 10) (Figures S1A–S1D). *Sox2* is not expressed in purified rod photoreceptors (FPKM < 1.0), so we performed co-immunolocalization with molecular markers of the other cell types and found that Sox2 is expressed in Müller glia and a subset of amacrine cells (Figures S1E–S1H). All 4 genes (*OKSM*) have H3K27me3 at their promoters and are hypomethylated in those regions (Figures 2J–2M). The promoter region for *Klf4* is the only one of the 4 genes with the H3K27Ac mark (Figure 2J). All 4 genes have H3K9me3 overlapping with the H3K27me3, and the ATAC-seq data are consistent with their epigenetic repression during differentiation (data available at https://pecan.stjude.org/proteinpaint/study/retina2017; Aldiri et al., 2017).

We have previously performed ChIP-seq analysis of purified rod photoreceptors (Aldiri et al., 2017); here, we extended those data to purified ON bipolar neurons from the *Grm6-GFP* transgenic mice (Dhingra et al., 2008) to gain insight into the epigenetic barrier to reprogramming. We performed ChIP-seq using previously validated antibodies for H3K27me3, H3K27Ac, H3K4me2, and H3K4me1. We compared the ChIP-seq for the 4 reprogramming genes between rods, bipolar neurons, and MEFs (Figures S2A–S2C) and found that the MEFs had more active histone marks (H3K27Ac, H3K4me2, and H3K4me1) and lacked the repressive histone mark (H3K27me3). The rods and bipolar neurons had much more H3K27me3 than the MEFs and fewer active marks (Figures S2A–S2C).

## Rod- and Bipolar-Derived iPSCs Have More Efficient Retinal Differentiation

To quantitate retinogenesis from each of our validated iPSC lines, we performed STEM-RET differentiation and scoring for 59 iPSC lines, as described previously (Figure 3A; Table S2) (Hiler et al., 2015, 2016). As a positive control, we used the EB5:Rx-GFP murine embryonic stem cell (ESC) line (Eiraku et al., 2011), and we also included fibroblast-derived iPSCs for our analysis (Table S2).

For eye field specification, we scored eye field induction efficiency (EFE), eye field induction specificity (EFS), and eye field proliferation (EFP) at day 7 (Figures 3A–3C; Table S2; Supplemental Information). For optic cup formation, we scored optic cup efficiency (OCE) and optic cup frequency (OCF) at day 10 (Figures 3A–3C; Table S2; Supplemental Information). To measure retinal differentiation (days 10–28), we analyzed 16 retinal differentiation genes by qPCR by using TaqMan probes and normalized them to *Gapdh* (retinal differentiation qPCR [RDQ]), 23 morphologic criteria by transmission electron microscopy (TEM [particularly, retinal differentiation electron microscopy; RDEM]), and 9 proteins by immunofluorescence on cryosections (retinal differentiation immunofluorescence; RDIF) (Figure 3C–3E; Table S2; Supplemental Information). Lines that failed to make retina were excluded from STEM-RET scoring but were analyzed in subsequent studies to elucidate epigenetic memory (discussed later). In total, 150 experiments were performed, and over 30,000 individual retinal spheres were scored using the STEM-RET protocol as described previously (Hiler et al., 2015, 2016).

There were significant differences in the STEM-RET scores across individual lines (Figures 3C–3H; Table S2). We also quantitated the proportion of retinal area in the organoids for retina produced from each retinal cell type and discovered that the retinal area was higher for lines that had higher STEM-RET scores (Figures 3C and 3F; Table S8; Supplemental Information). The best STEM-RET scores were achieved with the iPSC lines that were derived from the retinal cell types that were the most difficult to reprogram (rods and bipolar cells) relative to those that had more efficient reprogramming, such as amacrine/horizontal interneurons (Figures 3I–3K; Table S2).

## Epigenetic Memory of r-iPSCs

As expected, the RNA-seq profiles for each of the iPSC lines were very similar, because they are all fully reprogrammed multi-potent stem cells (Table S3). The lines did not cluster separately in principal-component analysis (PCA) of their gene expression profiles based on their cell of origin (Figures 4A and 4B) or their ability to make retina (Figure 4C). We identified the genes with significant differential gene expression (Table S3) across the 3 types of comparisons (retinal cell of origin, fibroblasts versus retinal origin, and ability to differentiate into retina) and performed pathway analysis. Most of the comparisons did not produce significant pathway enrichment ($q < 0.05$) (Table S4). However, the genes that were upregulated in rod-derived iPSCs relative to the other iPSC lines were enriched in chromatin binding, chromatin modification, and transcriptional regulation (Table S4).

To determine whether r-iPSCs retain an epigenetic memory of their cellular origins that is not necessarily reflected in their transcriptomes, we selected 33 lines for detailed epigenetic profiling (Table S1). We included iPSCs from each of the 5 retinal cell types, fibroblast-derived iPSCs, and the positive control EB5:Rx-GFP line. We also profiled 11 iPSC lines from diverse sources (retinal and fibroblast derived) that failed to make retina. We performed integrated analysis, including RNA-seq, DNA methylation analysis, and ChIP-seq of 8 histone marks (active chromatin: H3K4me1, H3K4me2, H3K4me3, H3K27Ac, H3K9/14Ac; repressed chromatin, H3K27me3 and H3K9me3; gene bodies: H3K36me3), as well as for CTCF, Brd4, and Pol II (Supplemental Information). All ChIP-seq was performed on

biological replicates, and all antibodies were independently validated for ChIP (protocols are available online at http://stjude. org/CSTN) (Aldiri et al., 2017). In total, 396 ChIP-seq libraries were sequenced for the 33 stem cell lines, and we compared their epigenetic profiles to normal developing mouse retina spanning 8 stages of development using the same approach (Aldiri et al., 2017). All data from ChIP-seq, DNA methylation, and RNA-seq are freely available in a searchable browser (https://pecan.stjude.org/proteinpaint/study/retinaliPSC2017).

Previous analysis of changes in DNA methylation with retinal differentiation identified upregulated and downregulated genes that had correlated and anticorrelated changes in DNA methylation in whole retina and in individual retinal cell types (Aldiri et al., 2017). Most of those genes were reset to the ESC state across iPSC lines from diverse sources (Table S5). For example, retinal progenitor genes such as *Pax6*, *Lhx2*, *Six3*, *Six6*, *Nes*, *Meis1*, and *Vsx2* had DNA methylation profiles that were reset to the ESC state in more than 95% of the iPSC lines (Figure 4D; Table S5). Similarly, many of the cell-type-specific retinal differentiation genes were efficiently reset to the ESC state in iPSCs. The rod-specific genes *Gnat1*, *Tulp1*, *Stx3*, *Prph*, and *Rpgr* were reset in over 95% of the iPSC lines (Table S5). However, there were some notable exceptions. *Nrl* was reset in 84% of the lines; *Prom1* and *Aipl1*, in 73% of the lines; *Rp1*, in 67% of the lines; *Pde6a*, in 50% of the lines; *Rho* and *Pde6b*, in 30% of the lines; and *Rcvrn*, *Guca1b*, and *Hk1*, in less than 16% of the lines (Figure 4E; Table S5).

Previous studies on the temporal changes in the epigenetic landscape during reprogramming have suggested that the first changes with reprogramming are the silencing of the cell-type-specific transcription program, followed by poised enhancers and heterochromatic regions enriched for the H3K9me3 repressive histone mark (Apostolou and Hochedlinger, 2013; Chronis et al., 2017). Using the previously published data on the dynamic epigenetic landscape during retinal development (Aldiri et al., 2017), we analyzed the efficiency of resetting of retinal cell-type-specific promoters and genes in our iPSC lines to the pluripotent state found in ESCs (Tables S6 and S7). Specifically, we performed Bayesian analysis of the chromHMM for each gene and promoter in each iPSC line to determine whether its epigenetic state was fully reset to the ESC state or whether it was a better match for one of the 9 developmental stages (embryonic day [E]14.5, E17.5, P0, P3, P7, P10, P14, P21, 11 months) with chromHMM data in the retina. There were retinal cell-type-specific genes such as *Aipl1* that were reset to the ESC pluripotent state in all 33 iPSC lines analyzed, regardless of their cellular origins (Figures 4F–4I; Tables S6 and S7). However, we also identified retinal-specific genes such as *Stx3* that failed to completely reset to the ESC pluripotent state in our iPSC lines and were a better match for the developing retina (Figures 4J–4M; Table S6). As noted earlier, *Stx3* reset to the ESC state in over 95% of iPSC lines based on DNA methylation, but there were differences in the resetting of the epigenome of *Stx3* to the ESC state that were revealed by the ChIP-seq analysis that was not evident in the DNA methylation analysis. Overall, the majority of cell-type-specific genes for rods (63%), cones (60%), Müller glia (69%), amacrine cells (62%), bipolar cells (64%), and ganglion cells (63%) reset to the ESC pluripotent state (Tables 1 and S6). Similar results were obtained for cell-type-specific promoters (Tables 1 and S7). For those that did not match the ESC state as well as the developing retina, the differences were often subtle, with

discrete regions of the gene or promoter having an epigenetic state that was a better match to retina than EB5:Rx-GFP ESCs (Figures 4J–4M).

Next, we analyzed the retinal enhancers and superenhancers identified previously (Aldiri et al., 2017), using the same Bayesian approach. The majority of retinal enhancers and superenhancers reset to the ESC pluripotent state (Figure S3; Tables 2 and S8). We analyzed the H3K9me3 regions of the genome, and they were reset at a similar efficiency (70%) as enhancers, superenhancers, genes, and promoters. However, retinal-specific heterochromatin predicted from the chromHMM (see Supplemental Information) was much less likely (20%–23% reset) to reset to the ESC state than active enhancers (72%–74% reset) or other regulatory regions (Table 2).

To determine whether the retinal-specific epigenetic memory was correlated with the ability of iPSCs to make retina, we compared the resetting efficiency of each class of genes, promoters, and enhancers in those iPSC lines that efficiently produce retina in 3D organoid cultures to the resetting efficiency in those lines that do not (Tables S6, S7, and S8). The retinal cell-type-specific genes, promoters, and enhancers were reset more efficiently in the iPSC lines that made retina relative to those that did not (Figures 4N and 4O), but there were no significant differences in the resetting of the broader chromatin domains (Figure 4P).

## Identification of a Biomarker for Retinal Differentiation in iPSCs

Genes encoding transcription factors that form core regulatory circuits (CRCs) often have cell-type-specific super-enhancers that contribute to a positive-feedback autoregulatory loop, and the same is true in stem cells (Saint-André et al., 2016). Using the CRC mapper (Saint-André et al., 2016) with our ChIP-seq data, we identified the core transcription factors in the iPSC lines used in our study. We also included EB5:Rx-GFP cells as a reference ESC line and several pre-iPSC lines from a previous publication (Chronis et al., 2017). Unsupervised hierarchical clustering revealed that 5 of the iPSC lines (rCh143.02, rG79.04, rCh257.4, rCr33.05, and FCR02) that did not make retina were more similar to the pre-iPSC lines in the CRC analysis than the EB5:Rx-GFP line (Figures 5A and 5B). Thus, by performing RNA-seq and H3K27Ac ChIP, and analyzing the CRCs, half of the iPSC lines that failed to make retina could have been prospectively identified from molecular analyses, even though immunofluorescent staining for stem cell markers, alkaline phosphatase staining, and teratoma formation was indistinguishable for these lines relative to the lines that efficiently made retina.

To determine whether the other epigenetic marks beyond H3K27Ac were useful in identifying iPSC lines that are defective in retinal differentiation, we analyzed each of the 11 individual histone marks and proteins from our ChIP-seq profiling at the promoters and in the gene bodies across all 33 lines. The most prominent difference was the elevated levels of H3K4me2 in the genes and promoters of iPSC lines that made retina relative to those that did not. Specifically, there were 186 genes and 739 promoters that had significantly elevated H3K4me2 in the lines that made retina relative to those that did not (Tables S9 and S10). For comparison, there were only 82 genes and 127 promoters that had differences in individual protein marks from ChIP-seq that correlated with the ability of lines to make retina for all the remaining marks combined (Tables S9 and S10). This was particularly striking because

of previous studies that have highlighted the importance of H3K4me2 in reprogramming (Barrero et al., 2013; Koche et al., 2011; Liang and Zhang, 2013). For example, studies on the temporal order of changes in histone modifications during reprogramming had indicated that there is a rapid genome-wide increase in H3K4me2 at thousands of loci early in reprogramming, such as the pluripotency genes and lineage-specific differentiation genes (Barrero et al., 2013; Koche et al., 2011; Liang and Zhang, 2013). While H3K4me2 is a histone modification associated with euchromatin, changes in H3K4me2 do not usually result in changes in gene expression. This is consistent with the lack of a strong transcriptional signature for iPSC lines that made retina versus those that did not in our analysis.

For each of the 739 promoters with elevated H3k4me2 in the iPSC lines that made retina, we further filtered to the top 121 promoters with an area under the curve (AUC) greater than 0.8 from receiver operating characteristic (ROC) curve analysis (Supplemental Information). We performed ChIP enrichment analysis (ChEA) (Lachmann et al., 2010) for the promoters and genes with elevated H3K4me2, and the top pathway was Meis1 target genes involved in optic cup formation (Table S11). The Meis1 target gene classification was also the top classification of the extended promoter list from the 739 genes with elevated H3K4me2 for the lines that made retina versus those that did not (Table S11). This was particularly interesting, because Meis1 is a homeodomain protein that is important for retinal development (Heine et al., 2008). *Meis1* expression was lower in iPSCs that made retina versus those that did not (Figures 5C and 5D), and this was reflected in the epigenetic profile (Figures 5E–5H). Specifically, H3K27me3 is present at the promoter of the *Meis1* gene in the EB5:Rx-GFP line and iPSC lines that efficiently make retina (Figures 5F and 5G), and the expression of *Meis1* in those lines was essentially undetectable (FPKM < 1.0). However, for a subset of lines that failed to make retina, they expressed *Meis1* and lacked the H3K27me3 histone modification at the promoter (Figure 5H). These data suggest that resetting of the Meis1 gene to the ESC epigenetic state revealed by ChIP-seq was not complete in all lines, and this had an impact on their ability to make retina.

To extend our analysis of the relationship between Meis1 expression and the ability of the retinal-derived iPSC line to differentiate into retina, we analyzed a group of iPSC lines that had not been previously analyzed. We found that 4 of the 8 iPSC lines in this group that failed to make retina had high levels of expression of *Meis1*, as measured by qPCR (Figure 5I). In total, 41 lines that made retina had levels of *Meis1* expression that were less than 50% of the levels found endogenously in the adult retina. Among the 16 lines that failed to make retina, 31% (5/16) had levels of *Meis1* expression similar to that of adult retina (Figure 5I).

The remaining 5 lines that failed to make retina and clustered with normal ESCs in the CRC analysis were outliers for individual epigenetic marks. Line rCh209.4 is an outlier for H3K36me3 (Figure 5J); rM0408, rCr263.4, andFCR01 are outliers for Pol II; and fG140.02 is an outlier for H3K4me1 (Figure 5J; data not shown). DNA methylation was less informative for identifying iPSC lines that failed to make retina in our analysis (Table S5; data not shown). Taken together, our data highlight the importance of performing integrated analysis with RNA-seq, DNA methylation profiling, and ChIP-seq to study epigenetic memory and to prospectively identify lines that will efficiently produce retina.

## DISCUSSION

In this study, we reprogrammed retinal neurons and Müller glia and discovered that there are cell-type-specific differences in reprogramming efficiency. While this may be due in part to the epigenetic landscape and nuclear organization of individual classes of retinal neurons, there are likely to be additional factors that contribute to differences in reprogramming efficiency. We also compared two different developmental stages for each of the 5 cell types. For those cell types that were more difficult to reprogram (rods and bipolar neurons), the immature cells were more readily reprogrammed than their mature fully differentiated counterparts. In order to relate the reprogramming efficiency to differentiation, we carried out retinal differentiation using a quantitative assay called STEM-RET (Hiler et al., 2015, 2016). Using this approach, we discovered that the lines derived from those cells that were more difficult to reprogram had better STEM-RET scores than iPSC lines derived from cells that had higher reprogramming efficiencies. Subsequent epigenetic profiling indicated that this was due to retention of epigenetic memory primarily made up of repressive marks. Taken together, these data suggest that there is an inverse correlation between reprogramming efficiency and epigenetic memory. Our study also identified a set of biomarkers, including *Meis1* and CRCs, that can be used to prospectively identify stem cell lines with the ability to make retina. Additional studies will be required to determine whether this extends to human iPSCs that may, one day, be used for cell-based therapy to treat retinopathies.

### Reprogramming Efficiency in the Retina

In order to quantitate the reprogramming efficiency of retinal cell types at different stages of development, we took advantage of the *Col1a1-OKSM;Rosa26-M2rtTA* reprogrammable mouse strain (Stadtfeld et al., 2010). The advantage of this mouse strain is that OKSM can be induced with the addition of doxycycline in a uniform manner with temporal control. We purified individual reprogrammable retinal cell types by flow sorting and then mixed them with an excess of non-reprogrammable retinal cell types to ensure that they survive during the 10 days of reprogramming in retinal pellet cultures, as described previously (Hiler et al., 2015, 2016). This is important, because previous studies on cortical neurons showed that they could not be reprogrammed when plated on plastic without the inactivation of p53. Our chimeric pellet cultures allowed us to reprogram retinal neurons without the inactivation of p53 and to provide a direct comparison across cell types and developmental stages.

Our data suggest that there are differences across cell types that are consistent with reprogramming efficiency. For example, rods are difficult to reprogram, and they have the highest proportion of heterochromatin (Figure 2C), lack endogenous expression of any of the reprogramming genes (Figure S1), and have *Myc* sequestered in the f-heterochromatin domain (Figures 2E and 2F). In contrast, cell types that are easy to reprogram, such as Müller glia and a subset of amacrine interneurons, have a lower proportion of their nuclear volume sequestered into heterochromatin (Figure 2C) and express the Sox2 protein (Figure S1). However, these data do not explain all aspects of the differences in reprogramming efficiency. Specifically, bipolar neurons have the highest proportion of euchromatin in their nuclei, but they have the lowest reprogramming efficiency. It is possible that there are other

aspects of genomic organization or other cellular features of bipolar neurons that make them difficult to reprogram using our mosaic pellet culture approach.

## Retinal Differentiation from r-iPSCs

In this study, we showed that virtually all r-iPSCs were equivalent in terms of the cell types produced, whether they were from immature or mature neurons or glia. In our previous study, we showed that the retina produced from iPSCs made from fibroblasts had specific defects in production of some retinal cell types (Hiler et al., 2015, 2016). While the r-iPSCs made intact retina, there were differences in the efficiency of retinal differentiation, as measured using the STEM-RET scoring system that incorporates quantitative measures of molecular and cellular features characteristic of eye field specification, optic cup formation, and retinal differentiation (Hiler et al., 2015, 2016). The mature rods and immature bipolar neurons had the lowest reprogramming efficiency, yet they had the highest STEM-RET score. Taken together, these data suggest that there is both positive and negative epigenetic memory in iPSCs. The positive epigenetic memory is present in the rod- and bipolar-derived iPSCs, and the negative epigenetic memory is present in the f-iPSCs.

The implication of this study is important in considering the cell source for reprogramming. If whole retina were used, those cells with the greatest propensity for reprogramming would be the ones most likely to produce iPSCs clones. As a result, the subsequent retinal differentiation would be somewhat less efficient. Instead, by performing comprehensive profiling of the individual cell types, it is possible to identify those cell types that produce the iPSCs that make the best retina. In the retina, the cell types that are most difficult to reprogram made the best retina, but additional studies on other regions of the CNS or other tissue would be required to determine whether the inverse relationship between reprogramming efficiency and differentiation is a general property of iPSCs or unique to the retina.

## Retinal Epigenetic Memory

We found that those retinal-specific genes and enhancers that undergo changes in their epigenetic state during development (Aldiri et al., 2017) were most likely to be properly reset to the native state found in ESCs. In contrast, the regions of the genome that were in more repressed epigenetic states and sequestered in heterochromatin in a cell-type-specific manner were the regions most likely to be retained in the iPSCs from retinal cell types. This was more prevalent in the iPSCs that were derived from cells that were most difficult to reprogram (rods and bipolar cells). These data are consistent with previous studies on the OKSM-mediated reprogramming of fibroblasts into iPSCs that suggested that there is a stepwise process that involves silencing of the cell-type-specific differentiation genes, resetting of poised enhancer elements, and reorganization of heterochromatin to the pluripotent state (Apostolou and Hochedlinger, 2013; Koche et al., 2011; Lister et al., 2011; Polo et al., 2012; Soufi et al., 2012). More recently, it was shown that Oct4, Sox2, and Klf4 target active enhancers early in the reprogramming process and redistribute cell-type-specific transcription factors (Chronis et al., 2017). Incomplete resetting of the epigenetic state can lead to epigenetic memory of the cellular origin for individual iPSC lines that, in turn, can impact subsequent lineage-specific differentiation. DNA methylation changes are

thought to occur last during the reprogramming process, and as a result, epigenetic memory is often reflected in the DNA methylation of iPSCs (Lister et al., 2011). Our data are consistent with those mechanisms and show that the histone modifications associated with heterochromatin are also an important component of epigenetic memory. However, we also discovered that there are genes that appear to reset completely to the ESC state by DNA methylation but had incomplete resetting of other epigenetic marks. To gain a more complete understanding of epigenetic memory in iPSCs, it may be important to include ChIP-seq and other methods to profile the epigenome in future studies on epigenetic memory.

### Biomarkers to Predict Retinal Differentiation

One of the major challenges in retinal differentiation of iPSCs is the prospective identification of lines that have the highest likelihood of making retina. In this study, we identified a set of stem cell lines that were fully reprogrammed but failed to make retina. They were indistinguishable from the lines that made retina, using standard assays for measuring pluripotency. However, using our STEM-RET protocol, they failed at the very early stage of eye field specification. We discovered that *Meis1* expression and the epigenetic state of *Meis1* and its target genes were useful markers of retinal potential in a subset of 30%–50% of iPSC lines. It is important to emphasize that this link between *Meis1* and retinal differentiation is counter-intuitive. One might assume that retaining expression of *Meis1* would promote retinogenesis, as it is required for early retinal development. However, the opposite was true. One explanation for this observation is that formation of the retina is a stepwise process in iPSC-derived organoids as it is *in vivo*, and expression of *Meis1* before it is required for eye field specification disrupts the entire process. Indeed, the lines that fail to make retina are defective in the earliest stages of retinal differentiation, consistent with the hypothesis that they fail to successfully transition through the requisite anterior neural specification. These data may also inform efforts to directly transdifferentiate fibroblasts or other cell types to retinal neurons. That is, it may be much more difficult to directly produce retinal neurons from fibroblasts if the cells do not transition through the key steps of early neurogenesis before retinal specification.

In addition to Meis1, CRC analysis was very helpful in identifying lines that were not fully reprogrammed from an epigenetic state, even though they met standard molecular and cellular criteria for reprogramming. At a minimum, H3K27Ac ChIP-seq and RNA-seq are required for CRC analysis, so by performing those two assays, the elevated *Meis1* and CRC analysis could be performed and would prospectively identify the lines that are less likely to make retina.

## EXPERIMENTAL PROCEDURES

### Animals

All procedures were approved by the Institutional Animal Care and Use Committee at St. Jude Children's Research Hospital. The reprogrammable mouse strain (*Col1a1*-OKSM; *Rosa-26-M2rtTA* mice) (Stadtfeld et al., 2010) was crossed with five different GFP transgenic mouse strains, including *Nrl*-GFP mice (Hiler et al., 2015), *Chrnb4-GFP* mice

(Siegert et al., 2009), *Cralbp-GFP* mice (Vázquez-Chona et al., 2009), *Gad1-GFP* mice (Huckfeldt et al., 2009), and *Grm6-GFP* mice (Dhingra et al., 2008), to produce reprogrammable mouse strains with transgenes labeling specific types of retinal cells that could be isolated by fluorescence-activated cell sorting (FACS). C57BL/6J mice (Jackson Laboratory, 000664) were used for supporting cells in retinal explant cultures for retinal reprogramming. *CD-1 nude* mice (Jackson Laboratory) were used to test the pluripotency of stem cell lines by teratoma formation.

### Statistical Analysis

For differential analysis of RNA-seq, gene-based raw counts were analyzed by Voom after TMM. $Log_2$ fold change, t values, p values, and FDR (false discovery rate)-corrected p values were extracted from Voom results and provided with FPKM values and AUC (area under the ROC curve) values. For ChIP-seq, we extended reads to the estimated fragment size and counted read numbers for promoters (transcription start site [TSS] ± 2 kb) or genes (TSS − 2 kb to TES + 2 kb) and performed statistical analysis with Voom. Instead of FPKM, we provided counts per million (CPM). For gene enrichment analysis, p values were determined using Fisher's exact test requested from the Enrichr server, while q values (i.e., FDR-corrected p value) were determined using the Benjamini-Hochberg method for correction for multiple-hypothesis testing.

## Supplementary Material

Refer to Web version on PubMed Central for supplementary material.

## Acknowledgments

We thank Angela McArthur for editing the manuscript. This work was supported, in part, by Cancer Center Support (CA21765) from the NCI, grants to M.A.D. from the NIH (EY014867, EY018599, and CA168875), and ALSAC. M.A.D. was also supported by the Tully Family Foundation, the Peterson Foundation, and HHMI. The 3D EM was performed with assistance from the Cell and Tissue Imaging Shared Resource at St. Jude, and the FISH analysis was performed with assistance from the Cytogenetics Shared Resource at St. Jude.

## References

Aldiri I, Xu B, Wang L, Chen X, Hiler D, Griffiths L, Valentine M, Shirinifard A, Thiagarajan S, Sablauer A, et al. The dynamic epigenetic landscape of the retina during development, reprogramming, and tumorigenesis. Neuron. 2017; 94:550–568.e10. [PubMed: 28472656]

Aoi T, Yae K, Nakagawa M, Ichisaka T, Okita K, Takahashi K, Chiba T, Yamanaka S. Generation of pluripotent stem cells from adult mouse liver and stomach cells. Science. 2008; 321:699–702. [PubMed: 18276851]

Apostolou E, Hochedlinger K. Chromatin dynamics during cellular reprogramming. Nature. 2013; 502:462–471. [PubMed: 24153299]

Bar-Nur O, Russ HA, Efrat S, Benvenisty N. Epigenetic memory and preferential lineage-specific differentiation in induced pluripotent stem cells derived from human pancreatic islet beta cells. Cell Stem Cell. 2011; 9:17–23. [PubMed: 21726830]

Barrero MJ, Sese B, Kuebler B, Bilic J, Boue S, Martí M, Izpisua Belmonte JC. Macrohistone variants preserve cell identity by preventing the gain of H3K4me2 during reprogramming to pluripotency. Cell Rep. 2013; 3:1005–1011. [PubMed: 23545500]

Beagan JA, Gilgenast TG, Kim J, Plona Z, Norton HK, Hu G, Hsu SC, Shields EJ, Lyu X, Apostolou E, et al. Local genome topology can exhibit an incompletely rewired 3D-folding state during somatic cell reprogramming. Cell Stem Cell. 2016; 18:611–624. [PubMed: 27152443]

Chen X, Pappo A, Dyer MA. Pediatric solid tumor genomics and developmental pliancy. Oncogene. 2015; 34:5207–5215. [PubMed: 25639868]

Chronis C, Fiziev P, Papp B, Butz S, Bonora G, Sabri S, Ernst J, Plath K. Cooperative binding of transcription factors orchestrates reprogramming. Cell. 2017; 168:442–459.e20. [PubMed: 28111071]

Dhingra A, Sulaiman P, Xu Y, Fina ME, Veh RW, Vardi N. Probing neurochemical structure and function of retinal ON bipolar cells with a transgenic mouse. J Comp Neurol. 2008; 510:484–496. [PubMed: 18671302]

Dyer MA. Lessons from retinoblastoma: implications for cancer, development, evolution, and regenerative medicine. Trends Mol Med. 2016; 22:863–876. [PubMed: 27567287]

Eiraku M, Takata N, Ishibashi H, Kawada M, Sakakura E, Okuda S, Sekiguchi K, Adachi T, Sasai Y. Self-organizing optic-cup morphogenesis in three-dimensional culture. Nature. 2011; 472:51–56. [PubMed: 21475194]

Eminli S, Foudi A, Stadtfeld M, Maherali N, Ahfeldt T, Mostoslavsky G, Hock H, Hochedlinger K. Differentiation stage determines potential of hematopoietic cells for reprogramming into induced pluripotent stem cells. Nat Genet. 2009; 41:968–976. [PubMed: 19668214]

Hanna J, Saha K, Pando B, van Zon J, Lengner CJ, Creyghton MP, van Oudenaarden A, Jaenisch R. Direct cell reprogramming is a stochastic process amenable to acceleration. Nature. 2009; 462:595–601. [PubMed: 19898493]

Heine P, Dohle E, Bumsted-O'Brien K, Engelkamp D, Schulte D. Evidence for an evolutionary conserved role of homothorax/Meis1/2 during vertebrate retina development. Development. 2008; 135:805–811. [PubMed: 18216174]

Hiler D, Chen X, Hazen J, Kupriyanov S, Carroll PA, Qu C, Xu B, Johnson D, Griffiths L, Frase S, et al. Quantification of retinogenesis in 3D cultures reveals epigenetic memory and higher efficiency in iPSCs derived from rod photoreceptors. Cell Stem Cell. 2015; 17:101–115. [PubMed: 26140606]

Hiler DJ, Barabas ME, Griffiths LM, Dyer MA. Reprogramming of mouse retinal neurons and standardized quantification of their differentiation in 3D retinal cultures. Nat Protoc. 2016; 11:1955–1976. [PubMed: 27658012]

Huckfeldt RM, Schubert T, Morgan JL, Godinho L, Di Cristo G, Huang ZJ, Wong RO. Transient neurites of retinal horizontal cells exhibit columnar tiling via homotypic interactions. Nat Neurosci. 2009; 12:35–43. [PubMed: 19060895]

Kim K, Doi A, Wen B, Ng K, Zhao R, Cahan P, Kim J, Aryee MJ, Ji H, Ehrlich LI, et al. Epigenetic memory in induced pluripotent stem cells. Nature. 2010; 467:285–290. [PubMed: 20644535]

Kim J, Lengner CJ, Kirak O, Hanna J, Cassady JP, Lodato MA, Wu S, Faddah DA, Steine EJ, Gao Q, et al. Reprogramming of postnatal neurons into induced pluripotent stem cells by defined factors. Stem Cells. 2011; 29:992–1000. [PubMed: 21563275]

Koche RP, Smith ZD, Adli M, Gu H, Ku M, Gnirke A, Bernstein BE, Meissner A. Reprogramming factor expression initiates widespread targeted chromatin remodeling. Cell Stem Cell. 2011; 8:96–105. [PubMed: 21211784]

Krijger PH, Di Stefano B, de Wit E, Limone F, van Oevelen C, de Laat W, Graf T. Cell-of-origin-specific 3D genome structure acquired during somatic cell reprogramming. Cell Stem Cell. 2016; 18:597–610. [PubMed: 26971819]

Lachmann A, Xu H, Krishnan J, Berger SI, Mazloom AR, Ma'ayan A. ChEA: transcription factor regulation inferred from integrating genome-wide ChIP-X experiments. Bioinformatics. 2010; 26:2438–2444. [PubMed: 20709693]

Liang G, Zhang Y. Embryonic stem cell and induced pluripotent stem cell: an epigenetic perspective. Cell Res. 2013; 23:49–69. [PubMed: 23247625]

Lister R, Pelizzola M, Kida YS, Hawkins RD, Nery JR, Hon G, Antosiewicz-Bourget J, O'Malley R, Castanon R, Klugman S, et al. Hotspots of aberrant epigenomic reprogramming in human induced pluripotent stem cells. Nature. 2011; 471:68–73. [PubMed: 21289626]

Lowry WE, Richter L, Yachechko R, Pyle AD, Tchieu J, Sridharan R, Clark AT, Plath K. Generation of human induced pluripotent stem cells from dermal fibroblasts. Proc Natl Acad Sci USA. 2008; 105:2883–2888. [PubMed: 18287077]

Nishino K, Toyoda M, Yamazaki-Inoue M, Fukawatase Y, Chikazawa E, Sakaguchi H, Akutsu H, Umezawa A. DNA methylation dynamics in human induced pluripotent stem cells over time. PLoS Genet. 2011; 7:e1002085. [PubMed: 21637780]

Park IH, Zhao R, West JA, Yabuuchi A, Huo H, Ince TA, Lerou PH, Lensch MW, Daley GQ. Reprogramming of human somatic cells to pluripotency with defined factors. Nature. 2008; 451:141–146. [PubMed: 18157115]

Polo JM, Liu S, Figueroa ME, Kulalert W, Eminli S, Tan KY, Apostolou E, Stadtfeld M, Li Y, Shioda T, et al. Cell type of origin influences the molecular and functional properties of mouse induced pluripotent stem cells. Nat Biotechnol. 2010; 28:848–855. [PubMed: 20644536]

Polo JM, Anderssen E, Walsh RM, Schwarz BA, Nefzger CM, Lim SM, Borkent M, Apostolou E, Alaei S, Cloutier J, et al. A molecular roadmap of reprogramming somatic cells into iPS cells. Cell. 2012; 151:1617–1632. [PubMed: 23260147]

Saint-André V, Federation AJ, Lin CY, Abraham BJ, Reddy J, Lee TI, Bradner JE, Young RA. Models of human core transcriptional regulatory circuitries. Genome Res. 2016; 26:385–396. [PubMed: 26843070]

Siegert S, Scherf BG, Del Punta K, Didkovsky N, Heintz N, Roska B. Genetic address book for retinal cell types. Nat Neurosci. 2009; 12:1197–1204. [PubMed: 19648912]

Singh VK, Kalsan M, Kumar N, Saini A, Chandra R. Induced pluripotent stem cells: applications in regenerative medicine, disease modeling, and drug discovery. Front Cell Dev Biol. 2015; 3:2. [PubMed: 25699255]

Solovei I, Kreysing M, Lanctôt C, Kösem S, Peichl L, Cremer T, Guck J, Joffe B. Nuclear architecture of rod photoreceptor cells adapts to vision in mammalian evolution. Cell. 2009; 137:356–368. [PubMed: 19379699]

Soufi A, Donahue G, Zaret KS. Facilitators and impediments of the pluripotency reprogramming factors' initial engagement with the genome. Cell. 2012; 151:994–1004. [PubMed: 23159369]

Stadtfeld M, Maherali N, Borkent M, Hochedlinger K. A reprogrammable mouse strain from gene-targeted embryonic stem cells. Nat Methods. 2010; 7:53–55. [PubMed: 20010832]

Takahashi K, Tanabe K, Ohnuki M, Narita M, Ichisaka T, Tomoda K, Yamanaka S. Induction of pluripotent stem cells from adult human fibroblasts by defined factors. Cell. 2007; 131:861–872. [PubMed: 18035408]

Vázquez-Chona FR, Clark AM, Levine EM. Rlbp1 promoter drives robust Müller glial GFP expression in transgenic mice. Invest Ophthalmol Vis Sci. 2009; 50:3996–4003. [PubMed: 19324864]

Yu J, Vodyanik MA, Smuga-Otto K, Antosiewicz-Bourget J, Frane JL, Tian S, Nie J, Jonsdottir GA, Ruotti V, Stewart R, et al. Induced pluripotent stem cell lines derived from human somatic cells. Science. 2007; 318:1917–1920. [PubMed: 18029452]

## Highlights

- Retinal reprogramming efficiency is cell type and developmental stage specific
- Reprogramming efficiency is inversely correlated with retinal differentiation
- DNA/chromatin modifications and nuclear organization affect reprogramming efficiency
- Meis1 expression is a predictive biomarker of retinal differentiation of iPSCs

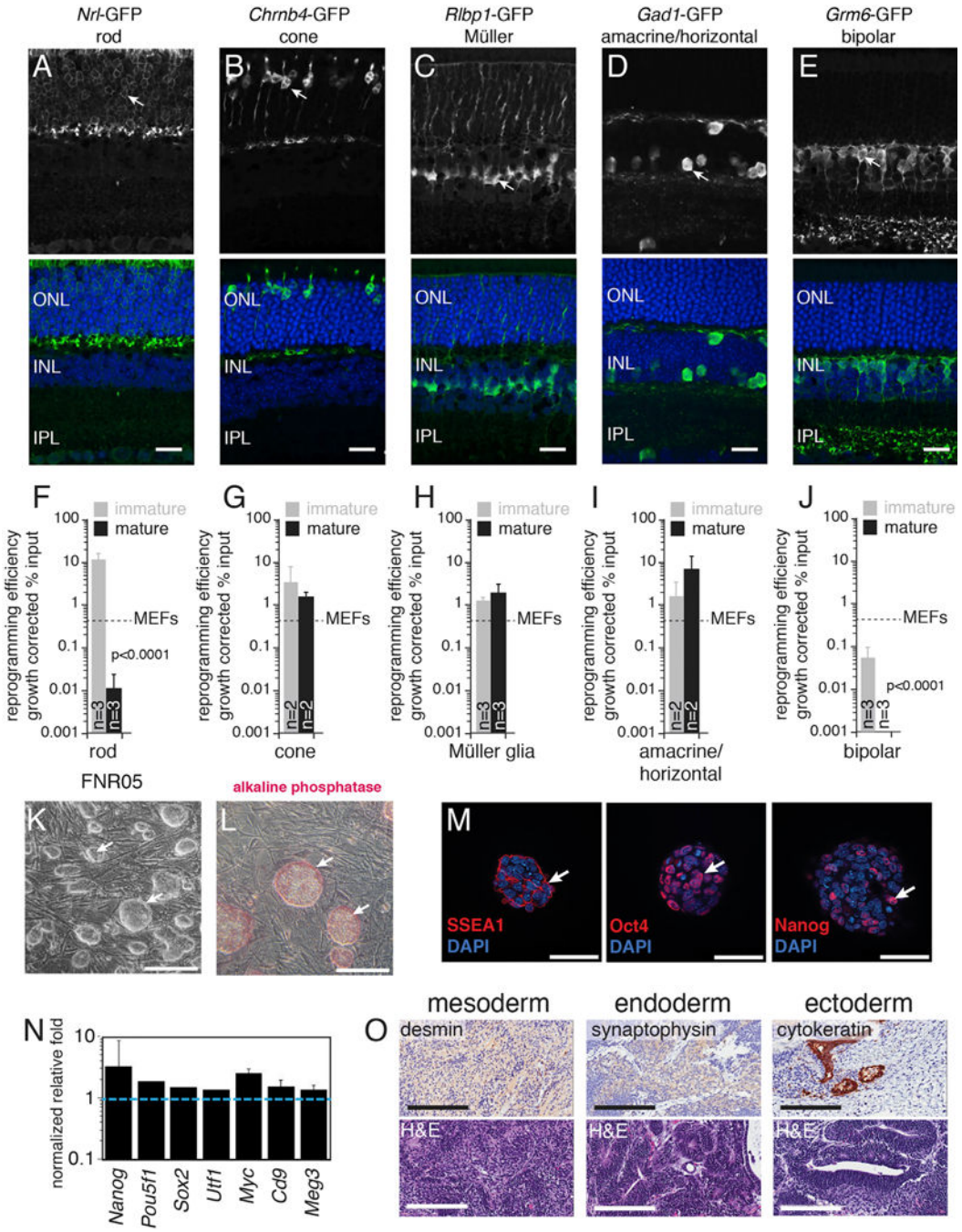


**Figure 1. Retinal Cell-Type-Specific Differences in Reprogramming**

(A–E) Micrographs of GFP expression alone (arrows in upper panels) and overlaid with DAPI (blue) in the lower panels. (A) *Nrl*-GFP rod; (B) *Chrnb4*-GFP cone; (C) *Rlbp1*-GFP Müller glia; (D) *Gad1*-GFP amacrine/horizontal cells; (E) Grm6-GFP bipolar cells.

(F–J) Bar charts of reprogramming efficiency for immature (gray) and mature retinal cell types. Each bar represents the mean and SD of biological replicate experiments as indicated. (F) Rod; (G) cone; (H) Müller glia; (I) amacrine/horizontal cells; (J) bipolar cells. The dashed lines indicate the reprogramming efficiency of mouse embryonic fibroblasts (MEFs).

Each of the retinal-derived cell types was significantly different from MEFs ($p < 0.001$), and there were significant differences between immature and mature rods ($p < 0.0001$) and bipolar neurons ($p < 0.0001$). The reprogramming efficiency is a growth-adjusted percentage of input (Supplemental Information), with number of experiments indicated on the bars.
(K) Micrograph of iPSC colonies after 20 passages on irradiated MEF feeder cells.
(L) Micrograph of alkaline-phosphatase-stained iPSC colonies (red).
(M) Micrograph of individual iPSC colonies immunostained for SSEA1, Oct4, and Nanog (red) with DAPI nuclear counterstain (blue).
(N) Bar chart of qPCR for 7 pluripotency genes plotted relative to the positive control cell line (EB5:Rx-GFP). Data are normalized to *Gapdh* and are plotted relative to EB5:Rx-GFP (blue dashed line). Each bar represents the mean and SD of technical replicate experiments for the iPSC clone shown in (K).
(O) Micrographs of immunohistochemical staining (upper panels) and H&E staining (lower panels) of representative teratoma made from r-iPSCs.
ONL, outer nuclear layer; INL, inner nuclear layer; GCL, ganglion cell layer. Scale bars, 25 μm in (A)–(E) and (M) and 100 μm in (K) and (L); and 200 μm in (O).
See also Table S1 and Supplemental Information.

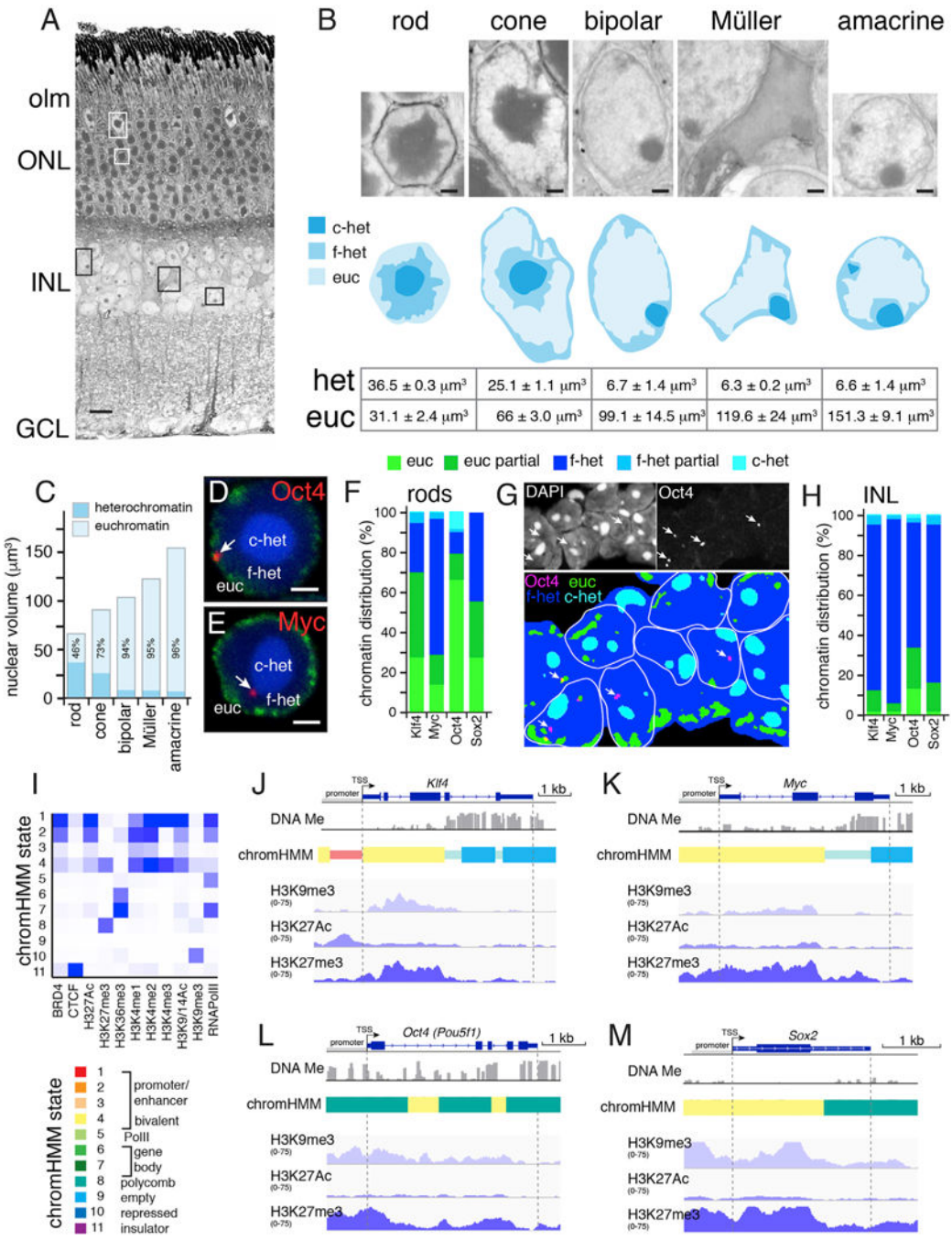


**Figure 2. Differences in Nuclear Organization across Retinal Cell Types**

(A) Electron micrograph of an adult mouse retina.

(B) Magnified regions from (A) in the upper panel and tracing of heterchromatin and euchromatin from those nuclei (blue). The mean and SD of the volume of heterochromatin and euchromatin was calculated from 3 individual nuclei for each cell type.

(C) Stack bar chart of nuclear volume distribution by cell type.

(D and E) Representative fluorescent *in situ* hybridization for (D) Oct4 and (E) Myc in mature rod nuclei (red) with the DAPI nuclear counterstain (blue) and immunofluorescence for H3K4me3 (green).
(F) Stack bar chart of the localization of each of the 4 reprogramming factors to rod nuclei, with a minimum of 50 nuclei scored per probe.
(G) Representative fluorescent *in situ* hybridization for Oct4 and Myc in mature inner nuclear layer (INL) nuclei (red) with the DAPI nuclear counterstain (blue) and immunofluorescence for H3K4me3 (green). The lower panel is the segmentation of each region using the machine learning algorithm developed for these studies.
(H) Stack bar chart of the localization of each of the 4 reprogramming factors to INL nuclei with a minimum of 50 nuclei scored per probe.
(I) Heatmap of the chromatin hidden Markov modeling (chromHMM) states. The chromHMM states are color coded below with the association to specific regions in the genome.
(J–M) Trace of DNA methylation, chromHMM, and ChIP-seq for H3K9me3, H3K27Ac, and H3K27me3 for each of the reprogramming genes in adult retina. The scale for the ChIP-seq is indicated for each mark. (J) *Klf4*; (K) *Myc*; (L) *Oct4 (Pou5f1)*; and (M) *Sox2*.
olm, outer limiting membrane; ONL, outer nuclear layer; INL, inner nuclear layer; GCL, ganglion cell layer; c-het, constitutive heterochromatin; f-het, facultative heterochromatin; euc, euchromatin. Scale bars, 10 μm in (A) and 1 μm in (B), (D), and (E).
See also Figures S1 and S2.

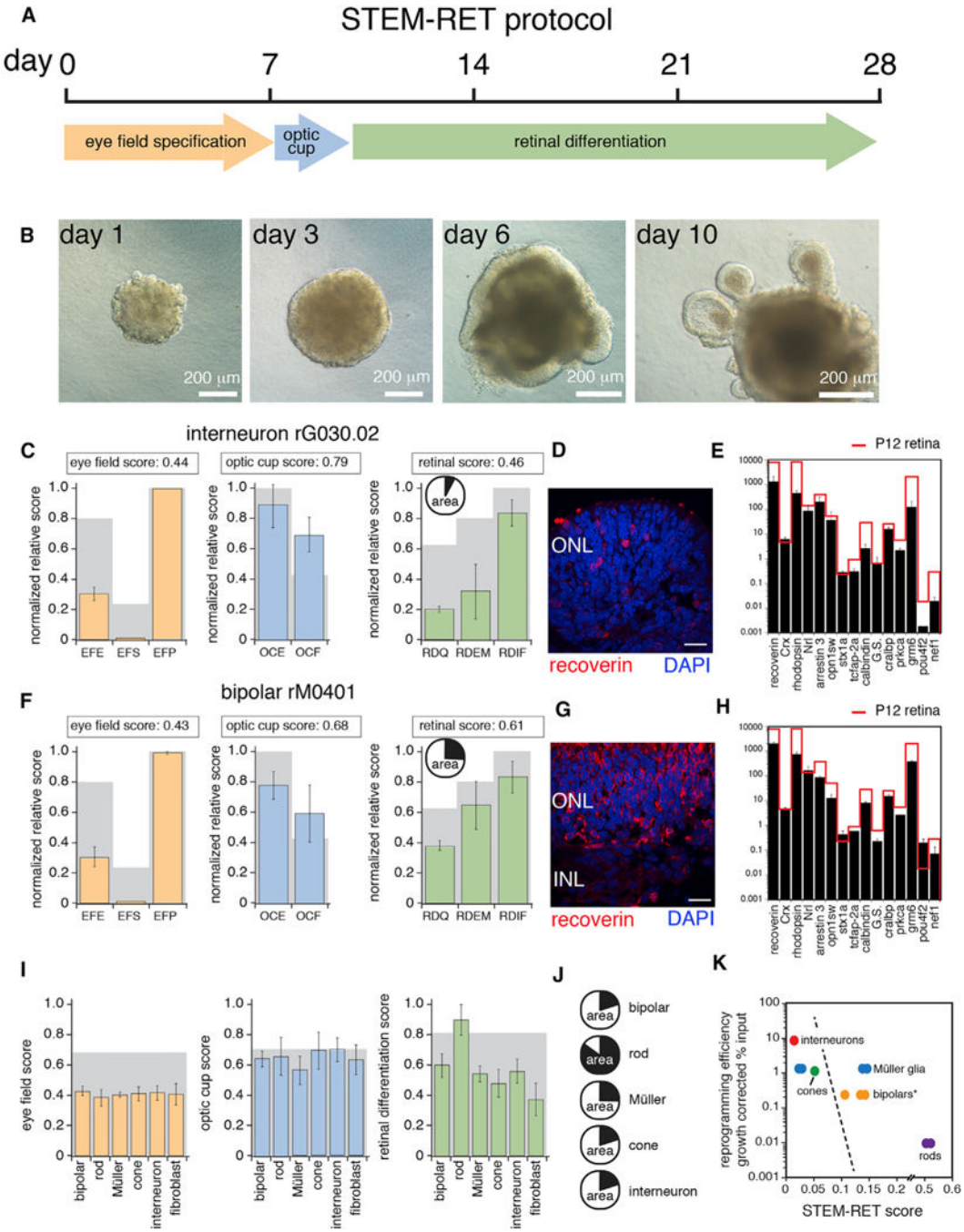


**Figure 3. R-iPSCs Have an Inverse Correlation between Reprogramming Efficiency and Retinal Differentiation**

(A) Outline of the STEM-RET protocol.

(B) Representative micrographs from several stages of STEM-RET differentiation.

(C) Bar chart of each scoring metric for a representative interneuron-derived iPSC line that has relatively poor performance in retinal differentiation. Each bar represents the mean and SD of at least 2 biological replicate experiments. The integrated scores for eye field, optic cup, and retinal differentiation are shown in the boxes. The gray bars represent the scores for

the positive control EB5:Rx-GFP line. The proportion of organoid that was retina based on triplicate experiments is shown.

(D) Micrograph of immunofluorescent staining of recoverin (red) and DAPI nuclear counterstain (blue).

(E) qPCR for 15 retinal differentiation genes relative to E14.5 retina. Each bar represents the mean and SD of 2 independent experiments, and normal P12 retina is shown in red.

(F) STEM-RET scores for a bipolar-derived iPSC line.

(G) Micrograph of recoverin staining for the rM0401 line shown in red, with DAPI nuclear counterstain (blue).

(H) qPCR for 15 retinal differentiation genes relative to E14.5 retina, as described above for (E).

(I) Combined eye field score, optic cup score, and retinal differentiation score for each cell type. Each bar represents the mean and SD of at least 4 lines per cell type in biological duplicates.

(J) Retinal area in organoids from each retinal-derived iPSC line. The mean is plotted from 3 independent experiments, and the SD is indicated in the supplemental tables Tables S1, S2, S3, S4, S5, S6, S7, S8, S9, S10, and S11.

(K) Plot of integrated retinal score including retinal area versus reprogramming efficiency. The dashed line separates the groups of iPSC lines that have significantly different reprogramming efficiency and retinal differentiation. The STEM-RET scores include retinal area calculations.

EFE, eye field efficiency; EFS, eye field specificity; EFP, eye field proliferation; OCE, optic cup efficiency; OCF, optic cup frequency; RDQ, retinal differentiation qPCR; RDEM, retinal differentiation electron microscopy; RDIF, retinal differentiation immunofluorescence. Scale bars, 200 μm in (B) and 25 μm in (D) and (G).

See also Tables S1, S2, S3, S4, S5, S6, S7, S8, S9, S10, and S11.

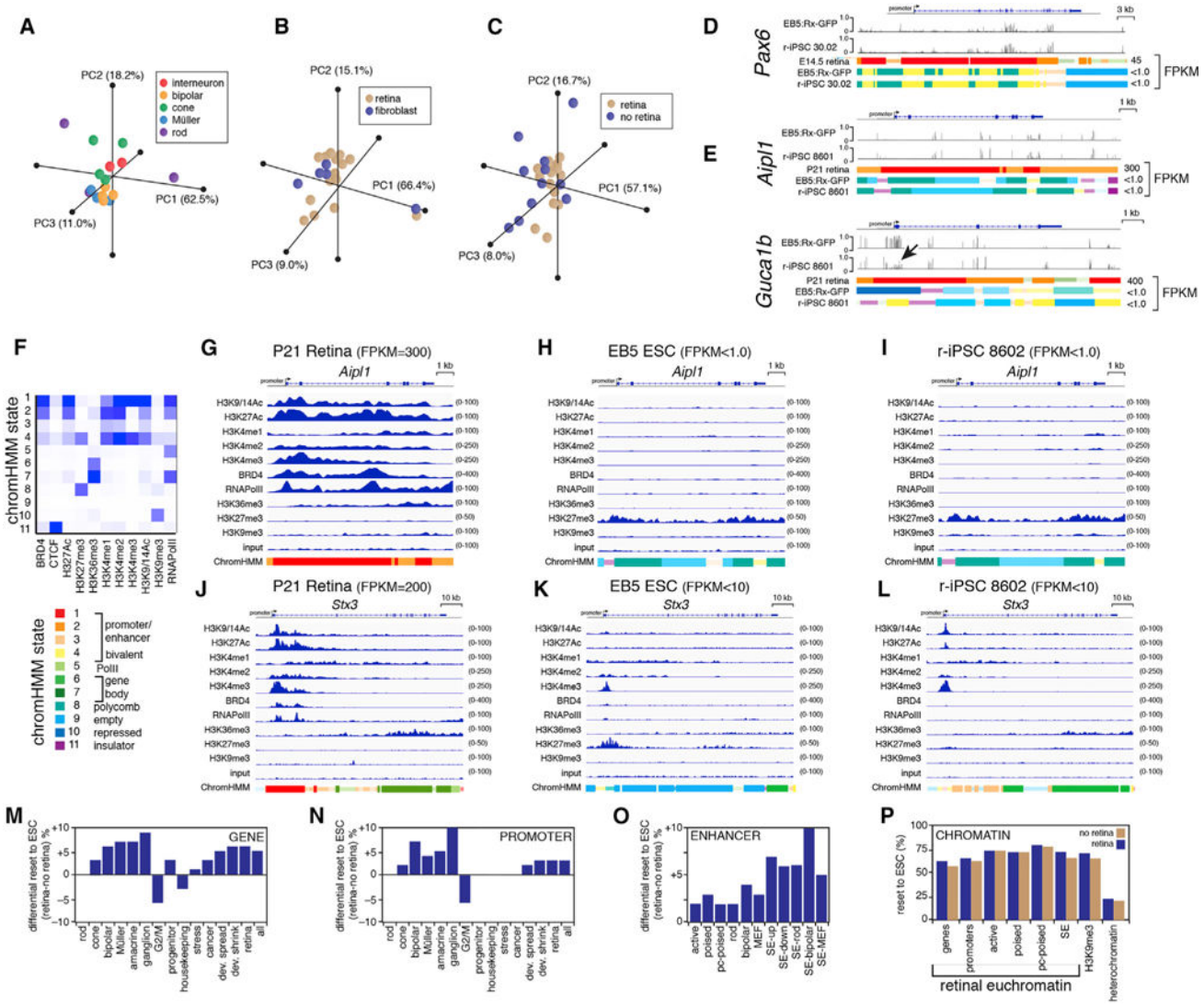


**Figure 4. Epigenetic Memory in R-iPSCs**

(A–C) Principal-component analysis of gene expression from RNA-seq for iPSCs derived from the different retinal cell types (A), comparing r-iPSCs to fibroblast-derived iPSCs (B), or comparing lines that made retina to those that did not (C).

(D) Representative examples of a progenitor gene that resets its DNA methylation profile to the EB5:Rx-GFP ESC state (*Pax6*).

(E) Representative example of a differentiation gene that resets the DNA methylation profile to the EB5:Rx-GFP ESC state (*Aipl1*) and one that did not (*Guca1b*). The arrow represents the region of differential DNA methylation.

(F) Heatmap of the chromatin hidden Markov modeling (chromHMM) states. The chromHMM states are color coded below with the association to specific regions in the genome.

(G–I) ChIP-seq tracks and chromHMM state for the *Aipl1* gene for the p21 retina (G), the EB5:Rx-GFP ESC line (H), and a representative retinal-derived iPSC line (I). The *Aipl1* gene was properly reset to the ESC state in the iPSC line.

(J–L) ChIP-seq tracks and chromHMM state for the *Stx3* gene in the p21 retina (J), the EB5:Rx-GFP ESC line (K), and a representative retinal-derived iPSC line (L). The retinal-derived iPSC line did not properly reset the H3K27me3 at the promoter of Stx3.
(M–O) Bar plot of the difference in percentage of iPSC lines that make retina versus those that failed to make retina for genes of each indicated category along the x axis (M). A similar plot is shown for the promoters of each gene class (N) or enhancer class (O). Each bar is the average of all genes across all lines.
(P) Bar plot of the percentage of genes or chromatin regions that reset to the ESC state for the lines that made retina versus those that failed to make retina. Each bar represents the average of all genes across all lines.
SE, superenhancer.
See also Tables S3 and S4.

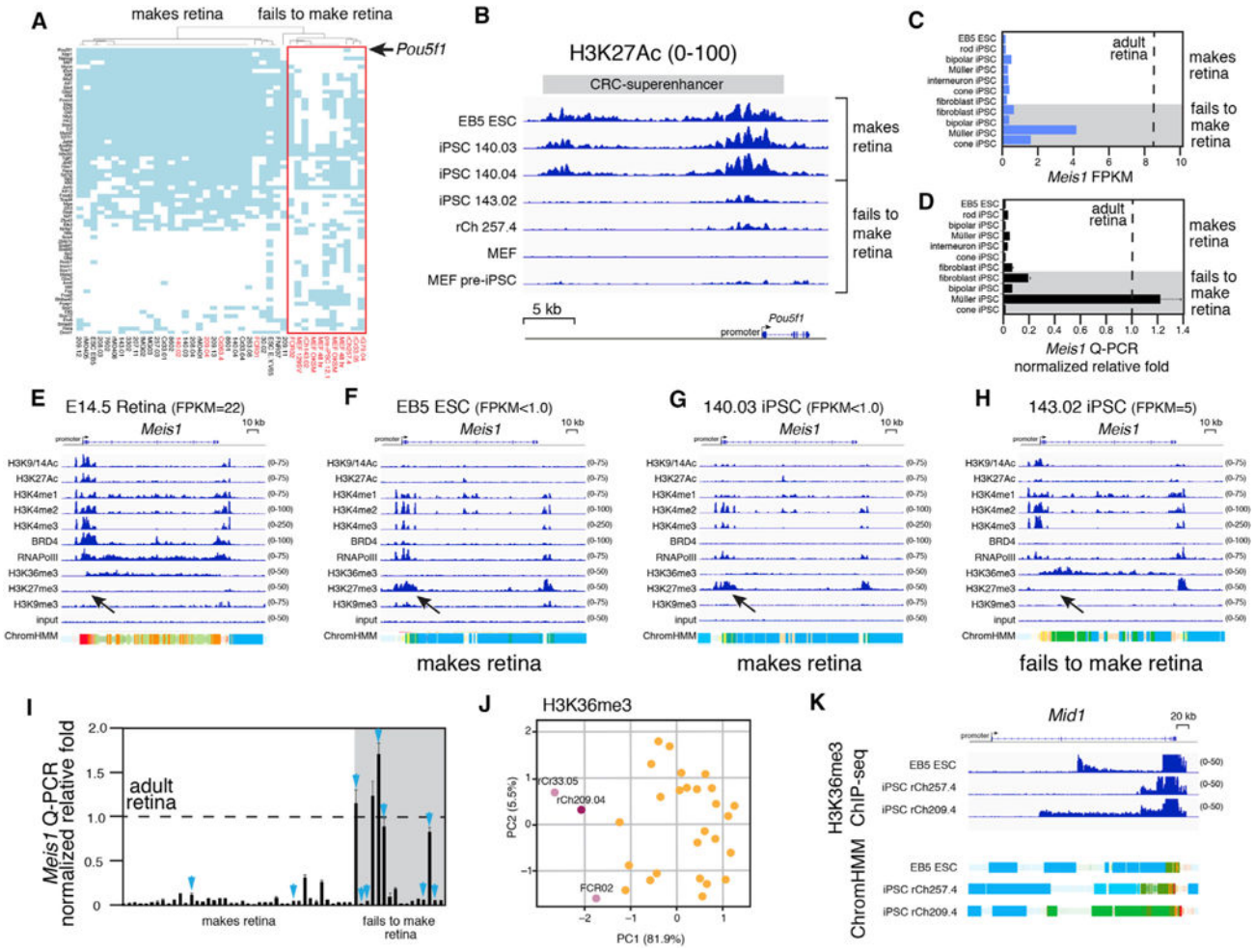


**Figure 5. Prospective Identification of iPSC Lines with the Potential to Make Retina in 3D Organoids**

(A) Heatmap of unsupervised hierarchical cluster of core regulatory circuit (CRC) analysis for all iPSC lines in this study, EB5:Rx-GFP ESCs, MEFs, and pre-iPSCs from MEFs. Blue indicates that the gene is a CRC in that cell line. The red box indicates a separate cluster with iPSC lines that fail to make retina (red).

(B) Representative ChIP-seq for the superenhancer for *Pou5f1* from the CRC heatmap in (A) showing that *Pou5f1* is a CRC gene in the ESCs, and two lines that make retina but did not reset to the ESC state in two lines that failed to make retina. Those lines had the CRC and ChIP-seq profile of MEFs and pre-iPSCs.

(C and D) Bar chart of RNA-seq (C) and qPCR for Meis1. A subset of the lines that failed to make retina (gray) had elevated levels of *Meis1* expression (D). Each bar in (D) represents the mean and SD of triplicate PCR reactions for the same cDNA sample. The dashed lines indicate the expression of *Meis1* in adult mouse retina.

(E–H) ChIP-seq and chromHMM of the Meis1 gene for E14.5 mouse retina when the gene is expressed at its peak (E), the EB5:Rx-GFP ESC line (F), an iPSC line that makes retina and has low expression of *Meis1* (G), and an iPSC line that fails to make retina (H). Arrows indicate a major peak of H3K27me3 at the promoter of the *Meis1* gene.

(I) Bar chart of qPCR for *Meis1* for 40 iPSC lines that make retina and 16 lines that fail to make retina (gray box). The blue arrows indicate independent lines that were used as a validation cohort for *Meis1* expression to predict lines that fail to make retina. The dashed line indicates the expression of *Meis1* in adult mouse retina.
(J) PCA plot of H3K36me3 in genes across 29 iPSC lines. The light red dots indicate samples that are outliers in this PCA, and the dark red dot indicates a sample that was not identified in previous CRC analysis or *Meis1* expression analysis. The yellow/orange dots indicate the individual iPSC lines that are similar in this PCA.
(K) ChIP-seq for H3K36me3 and chromHMM for EB5:Rx-GFP ESCs, an iPSC line that makes retina (rCh257.4), and an iPSC line that fails to make retina (rCh209.4).
See also Tables S9, S10, and S11.

**Table 1**

Proportion of Genes and Promoters that Reset to the ESC State in iPSC Lines

| | Gene Reset | | | Promoter Reset | | |
|---|---|---|---|---|---|---|
| **Group** | **Total (%)[a]** | **Retina (%)[b]** | **No Retina (%)[c]** | **Total (%)[a]** | **Retina (%)[b]** | **No Retina (%)[c]** |
| Rod | 63 | 63 | 63 | 64 | 64 | 64 |
| Cone | 60 | 61 | 57 | 62 | 62 | 62 |
| Bipolar | 64 | 66 | 60 | 68 | 70 | 63 |
| Müller | 69 | 71 | 64 | 57 | 58 | 54 |
| Amacrine | 62 | 64 | 57 | 63 | 65 | 60 |
| Ganglion | 63 | 67 | 56 | 64 | 67 | 57 |
| G2/M | 57 | 55 | 61 | 70 | 68 | 74 |
| Progenitor | 63 | 64 | 61 | 61 | 61 | 61 |
| Housekeeping | 59 | 58 | 61 | 68 | 68 | 68 |
| Stress | 54 | 54 | 53 | 64 | 64 | 64 |
| Cancer | 56 | 57 | 54 | 64 | 63 | 63 |
| Dev. spread | 69 | 71 | 66 | 72 | 73 | 71 |
| Dev. shrink | 62 | 64 | 58 | 62 | 63 | 60 |
| Retina | 61 | 63 | 57 | 64 | 65 | 62 |
| All | 60 | 60 | 55 | 62 | 63 | 60 |

See also Tables S5, S6, and S7.

[a]The percentage is indicated for all 33 iPSC lines.

[b]The percentage is indicated for the iPSC lines that make retina.

[c]The percentage is indicated for the iPSC lines that did not make retina.

**Table 2**

Proportion of Enhancers that Reset to the ESC State in iPSC Lines

| Group | Reset Total (%)[a] | Reset Retina (%)[b] | Reset No Retina (%)[c] |
|---|---|---|---|
| Active | 73 | 74 | 72 |
| Poised | 72 | 73 | 70 |
| PC-poised | 79 | 79 | 77 |
| Rod | 65 | 66 | 64 |
| Bipolar | 70 | 71 | 67 |
| MEF | 74 | 74 | 71 |
| SE-up | 70 | 72 | 65 |
| SE-down | 61 | 62 | 56 |
| SE-rod | 67 | 69 | 63 |
| SE-bipolar | 61 | 64 | 54 |
| SE-MEF | 53 | 54 | 49 |
| H3K9me3 | 70 | 72 | 66 |
| Heterochrom. | 22 | 23 | 20 |

See also Figure S3 and Table S8. heterochrom., heterochromatin.

[a]The percentage is indicated for all 33 iPSC lines.

[b]The percentage is indicated for the iPSC lines that make retina.

[c]The percentage is indicated for the iPSC lines that did not make retina.